


Preparation of pavement base material by using steel slag powder and steel slag aggregate

Mengmeng Fan^{1,2}, Zhengfan Lyu^{1,2} , Li Liu³, Jinxi Qin⁴, Gaorong Liang¹, Ningjie Huang⁵

¹Guangxi Jiaojian Engineering Inspection Consulting Co., Ltd. 530001, Nanning, China.

²Nanning Road Construction Technology and Road Construction Materials Engineering Technology Research Centre. 530001, Nanning, China.

³Changsha University of Science and Technology, School of Traffic and Transportation Engineering. 410114, Changsha, China.

⁴Guangxi Xinfazhan Communication Group Co., Ltd. 530001, Nanning, China.

⁵Guangxi Road Construction Engineering Group Co., Ltd. 530001, Nanning, China.

e-mail: fanmengmeng1712@163.com, lyuzhengfan@foxmail.com, 805296712@qq.com, 1652603363@qq.com, 2360337954@qq.com, 465624109@qq.com

ABSTRACT

The extensive use of cement has caused significant resource consumption and serious carbon emission problems. Recycling steel slag to partially replace cement presents a promising alternative. This study utilized steel slag powder (SSP) and steel slag aggregate (SSA) to prepare cement stabilized aggregate (CSA). The effects of different amounts of SSP and SSA on the road performance of CSA were studied, which was also compared with cement-fly ash (FA) stabilized aggregate (CFSA). The results demonstrated that adding SSP and SSA resulted in higher optimal moisture content and the maximum dry density of CSA. Adding 10% SSP enhances the mechanical properties of CSA. Compared to FA, SSP shows superior improvement effects at a 30% substitution rate. The dry shrinkage coefficient of CSA decreases as the SSP content increases. Further addition of SSA can further reduce shrinkage of CSA. The proper amount of SSP has no obvious effect on cement hydration, and the hydration degree of cement-SSP was higher than that of cement-FA. In addition, the higher the SSP blend, the lower the cost of the CSA and the lower the carbon emissions. Taking into account the performance, environmental impact, and cost of CSA, the optimal admixture of SSP is 30%.

Keywords: Steel slag; Steel slag powder; Cement stabilized aggregate; Road performance; Microanalysis.

1. INTRODUCTION

Steel slag (SS) is a solid waste produced in the steel smelting process. According to the 2022 national crude steel production data published by the National Bureau of Statistics of China, China's steel slag production is projected to 132 million tons in 2022 alone [1]. However, the comprehensive utilization rate of steel slag in China remains below 30% [2]. Large stockpiles of SS not only occupy valuable land resources but also cause a series of environmental pollution and human health problems [3, 4]. Therefore, achieving efficient resource utilization of steel slag has become a current research hot spot.

SS has potential cementitious activity. The main chemical compositions of SS are CaO, Fe₂O₃, SiO₂, and MgO [5], which have the same reactive minerals as cement, such as C₂S and C₃S [6]. Therefore, it can be used for the production of steel slag cement [7, 8], or directly applied in fields such as building materials, cement-based materials, and concrete [9–12]. For example, ZHUO *et al.* [13] found that steel slag powder (SSP) contains active substances such as calcium oxide and alumina. Adding an appropriate amount of SSP to slag powder-cement-based concrete can effectively improve the interfacial bonding performance between cement-based slurry and aggregate, as well as the fracture performance of concrete. TIAN *et al.* [14] found that the carbonation resistance of pavement concrete increased with the increase of SSP, and the addition of 15% SSP can achieve the best impermeability and frost resistance of pavement concrete. In addition, SSP also has the effect of improving the compactness of concrete microstructure [15], and the introduction of SSP in self-compacting concrete (SCC) can also promote the freshness of SCC [16].

SS is also a potential aggregate resource due to its hard texture, high abrasion resistance, and high mechanical strength [17–19]. In this regard, DONDI *et al.* [19] added a certain amount of SSA to the asphalt mixture, resulting in higher stability and stiffness of the asphalt mixture. In SHEN *et al.*'s study [20], SSA exhibited better asphalt adhesion than diabase aggregate due to the chemical reaction between SSA and rubber asphalt. PALANKAR *et al.* [21] prepared an environmentally friendly alkali-activated slag concrete using SSA as a substitute for natural coarse aggregate. ALEX RAJESH *et al.* [22] found that adding SSA to concrete can enhance its splitting tensile strength. At the optimal dosage of 9%, the 28-day splitting tensile strength of the concrete increased by 22.6%. The results showed that the concrete still had similar strength to the controls (without SSA) at 50% SS substitution.

The above studies have shown that SSP can improve the properties of materials such as cementitious materials and concrete and that the use of SSA as an aggregate also has the effect of improving the properties of materials. However, there is still limited research on the application of SSP and SSA in the field of pavement base, and the relevant mechanism of action is not yet clear. In order to promote the resource utilization of SS, this paper applied SSP and SSA to CSA. The road performance of CSA containing SSP and SSA and the microscopic properties of SSP-containing cementitious slurry were mainly investigated to determine the feasibility of using SSP and SSA for the preparation of pavement base materials.

2. MATERIALS AND METHODS

2.1. Raw materials

The cement (OPC) is Chinese Portland cement (P·O 42.5), produced by Guangxi Yufeng Cement Company, with a specific surface area of $392 \text{ m}^2 \cdot \text{kg}^{-1}$. SSP is produced by Guangxi Yuan Sheng Slag Comprehensive Utilization Co., Ltd., with a specific surface area of $450 \text{ m}^2 \cdot \text{kg}^{-1}$. Fly ash (FA) is provided by a power plant in Guangxi with a specific surface area of $372 \text{ m}^2 \cdot \text{kg}^{-1}$. The mineral composition of the SSP and FA was analyzed by X-ray diffractometer (XRD) with results shown in Figure 1. The main mineral components in SSP are calcium hydroxide ($\text{Ca}(\text{OH})_2$), calcium carbonate (CaCO_3), tricalcium silicate (C_3S), dicalcium silicate (C_2S), RO phase, and dicalcium ferrite (C_2F), etc., and the main mineral components in FA are mullite phase ($3\text{Al}_2\text{O}_3 - 2\text{SiO}_2$), quartz (SiO_2), hematite (Fe_2O_3), and calcite (CaCO_3). The particle size distribution of OPC, SSP and FA was analyzed by a laser particle size distributor, as shown in Figure 2. The results indicate that SSP has the smallest particle size, FA has the largest, and OPC's particle size is intermediate between the two.

The chemical compositions of cement, SSP, and FA were determined using an X-ray fluorescence spectroscopy analyzer (XRF), as presented in Table 1. Other performance indicators of cement are shown in Table 2.

The common aggregate is limestone aggregate with grain sizes of 0–5 mm, 5–10 mm, 10–20 mm, and 20–30 mm respectively. The grain size of SS aggregate (SSA) is 5–10 mm. The technical specifications of the test aggregates are shown in Table 3 and Table 4 respectively. The results of the sieving tests are shown in Table 5.

2.2. Mix proportion

As shown in Table 6, the experiment designed CSA with 4%, 5%, and 6% cementitious materials content, using 0%, 10%, 30%, and 50% SSP as partial replacement of cement to determine the effect of the content of SSP on the performance of CSA. A set of CSA with 5% cementitious materials and 30% FA dosing was also set as a comparison to evaluate the performance of SSP. In addition, to study the effect of SSA on CSA, the content of cementitious material was fixed at 5%, and the content of SSP was 30%. And CSA was prepared by replacing 5–10 mm gravel with 5–10 mm SSA. Considering the large difference between the apparent density of SSA and crushed stone, which would lead to the deviation of the actual gradation from the design gradation, the volumetric method described in the reference [23] was used to replace the limestone with the equal volume of SSA.

2.3. Test method

The Proctor compaction test was conducted in accordance with the Chinese Standard JTG E51-2009 *Test Methods of Materials Stabilized with Inorganic Binders for Highway Engineering*. In this study, a large compaction mold with an inner diameter of 152 mm, a height of 170 mm, and a volume of 2177 mL was used. Five moisture content levels were set for each mix: 3%, 4%, 5%, 6%, and 7%. Each sample was compacted in three layers, with 98 compactions per layer. The compaction hammer weighed 4.5 kg, and the diameter of the hammer's striking face was 50 mm.

According to the Chinese Standard JTG E51-2009, cylindrical samples with a diameter and height of 150 mm were prepared by static pressure method. The samples were then placed in sealed bags and cured for 6 days at a temperature of $20^\circ\text{C} \pm 1^\circ\text{C}$ and a relative humidity of $\geq 95\%$. Subsequently, all samples were

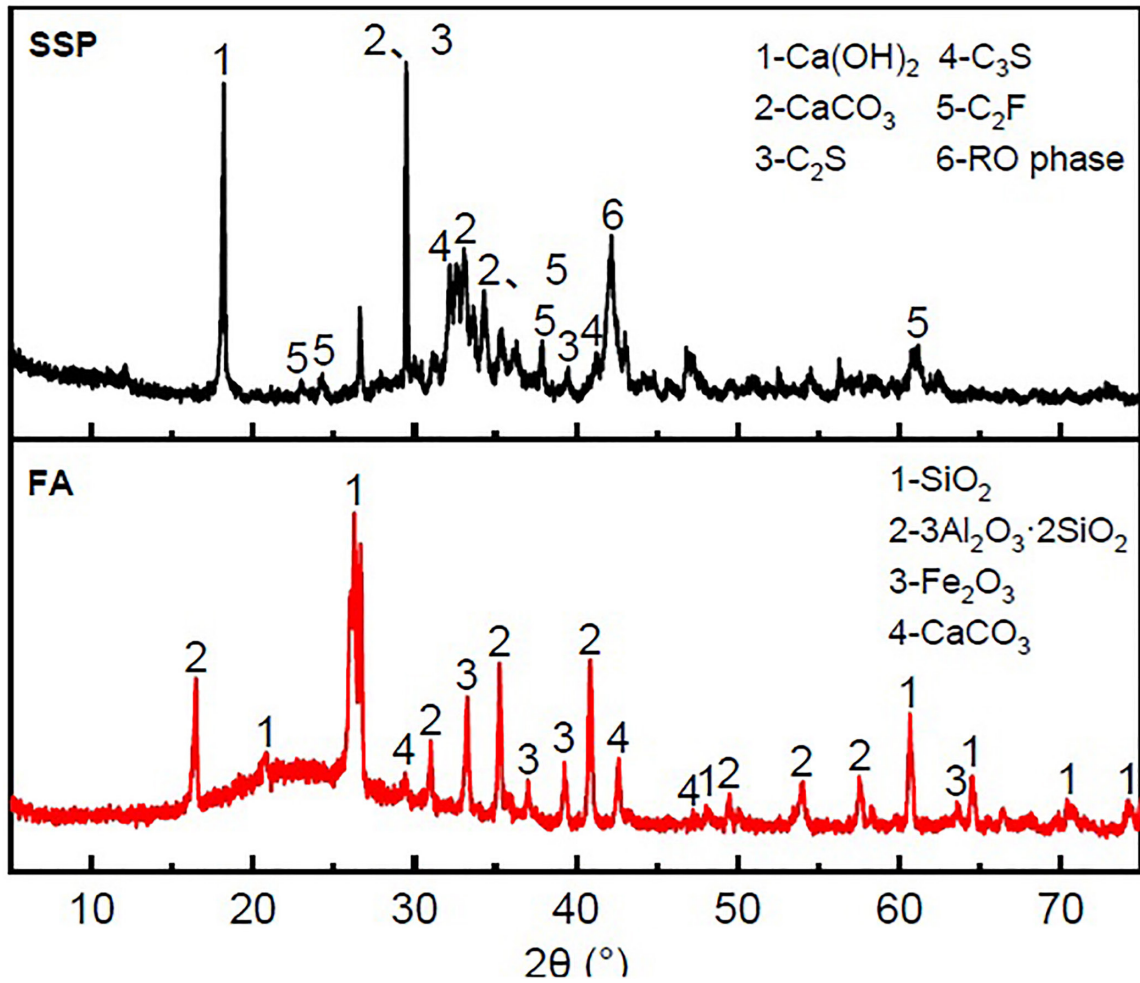


Figure 1: XRD spectrums of steel slag and fly ash.

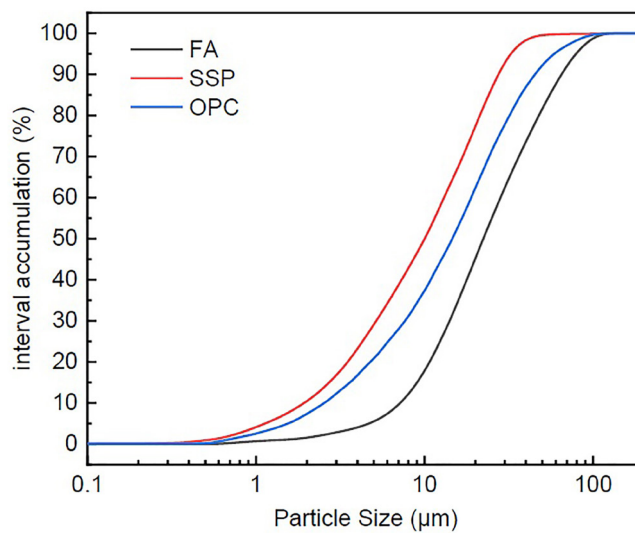


Figure 2: Particle size distribution curves of different raw materials.

immersed in water at a temperature of $20^{\circ}\text{C} \pm 1^{\circ}\text{C}$ and cured for 1 day. The unconfined compressive strength test was carried out at a loading rate of 1 mm/min after curing for 7d. The split tensile strength was performed with a loading rate of 1 mm/min after being cured for 90d. For both experiments, the arithmetic mean of 13 parallel tests was used as the result.

Table 1: Page dimensions for all text.

CHEMICAL COMPOSITION	Na ₂ O	Fe ₂ O ₃	Al ₂ O ₃	SiO ₂	CaO	TiO ₂	SO ₃	MgO	K ₂ O	MnO
OPC (%)	0.28	3.20	5.55	21.47	62.58	/	1.85	3.72	0.63	/
SSP (%)	0.31	19.70	4.83	17.65	40.90	0.87	/	6.66	/	4.61
FA (%)	0.31	6.29	28.23	50.81	3.87	/	/	1.20	0.62	/

Table 2: Cement performance indicators.

FINENESS (m ² ·kg ⁻¹)	NORMAL CONSISTENCY (%)	INITIAL SETTING TIME (min)	FINAL SETTING TIME (min)	28d COMPRESSIVE STRENGTH (MPa)	28d FLEXURAL STRENGTH (MPa)
364	26.8	165	284	61.5	7.7

Table 3: Technical indicators of coarse aggregate.

AGGREGATES SPECIFICATIONS	DENSITY (g·cm ⁻³)	CRUSHING VALUE (%)	WATER ABSORPTION (%)	NEEDLE-FLAKE CONTENT (%)	SOAKING EXPANSION RATE (%)
SSA (5~10 mm)	3.466	11.7	2.05	3.6	1.2
Gravel (5~10 mm)	2.715	13.9	0.57	8.8	0.4
Gravel (10~20 mm)	2.703	13.9	0.46	9.1	0.4
Gravel (20~30 mm)	2.705	13.9	0.34	9.0	0.4

Table 4: Technical indicators of fine aggregate.

AGGREGATES SPECIFICATIONS	CHLORIDE ION CONTENT (%)	SULPHATE CONTENT (%)	ALKALI-ACTIVE (%)	WATER ABSORPTION (%)	MICA CONTENTS (%)
Sand (0~5 mm)	0.005	0.22	0.025	0.66	0.4

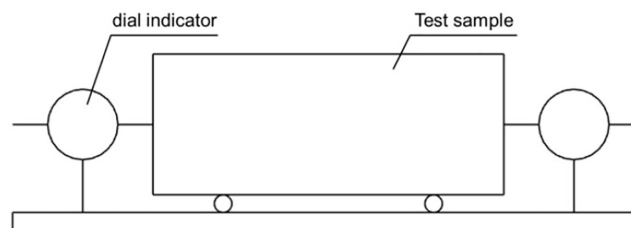
Table 5: Aggregate screening test results.

AGGREGATES SPECIFICATIONS	PASSING RATE/%						
	31.5 (mm)	19 (mm)	9.5 (mm)	4.75 (mm)	2.36 (mm)	0.6 (mm)	0.075 (mm)
Sand (0~5 mm)	100	100	100	99.3	79.7	42.4	8.1
SSA (0~5 mm)	100	100	80.9	10	3.3	3.1	2.2
Gravel (5~10 mm)	100	100	76.6	3.2	0.9	0.9	0.8
Gravel (10~20 mm)	100	100	99.8	31	1.4	1.3	1.3
Gravel (20~30 mm)	100	12.9	0.5	0.5	0.5	0.5	0.5

According to the Chinese Standard JTG E51-2009, samples with dimensions of 100 mm × 100 mm × 400 mm were made for the drying shrinkage test, placed on a shrinkage tester (Figure 3) after being cured for 7d, and tested in an environment at a temperature of 20°C ± 1°C and a relative humidity of 60% ± 5%. Each group consists of 6 samples, with 3 specimens used for measuring shrinkage deformation and the remaining 3 specimens used for measuring mass change. The test results are determined based on their respective arithmetic means. Record the readings of the dial gauge and the quality changes of the sample once a day within one week of the start of the experiment. The dial gauge readings and the sample's quality changes were recorded every

Table 6: Mix proportions.

TEST NUMBER	PROPORTION OF CEMENTITIOUS MATERIALS (%)			AGGREGATES PROPORTION (%)				
	CEMENT	STEEL SLAG POWDER	FLY ASH	0~5 mm SAND	5~10 mm GRAVEL	5~10 mm SSA	10~20 mm GRAVEL	20~30 mm GRAVEL
SS0	100	/	/	26	15	/	33	26
SS10	90	10	/			/		
SS30	70	30	/			/		
SS50	50	50	/			/		
FA30	70	/	30			/		
SS30G	70	30	/	25	/	15	34	26

**Figure 3:** Schematic diagram of shrinkage tester.

two days from the 7th to the 28th days and once within 60 days and 90 days respectively. Considering that the cement content of CSA used for road base is usually 5%, CAS with 5% cementitious material was selected for dry shrinkage performance testing.

The water-soaking swelling test was carried out according to the Chinese Standard GB/T 24175-2009 *Test Method for Stability of Steel Slag*. Firstly, the compacted samples were made by the optimum moisture content and maximum dry density, and a dial gauge was installed on the top of the compacted samples. The samples were then placed in a water bath (at 90°C) with a water level of 2.5 cm above the top surface of the sample and heated for 6h per day, and readings were taken before each heating for 10d. Finally, the average of three parallel tests is taken as the water-soaking expansion test result.

The mineral phases of CSA cementitious material net paste were analyzed using a D/MAX 2500V X-ray diffractometer (XRD) produced by Rigaku Corporation, Japan. The scanning range of XRD was set from 5° to 75° at a rate of 8°/min, employing an operating voltage of 40 kV and a current of 150 mA. The microscopic morphology of the skeletal structure of CSA cementitious material net paste was observed using an S-3400N scanning electron microscope (SEM) produced by Hitachi Limited, Japan. The operating voltage of SEM was set at 15 kV and the magnification at 2000 times.

3. RESULTS AND DISCUSSION

3.1. Proctor compaction test

Figure 4 shows the results of the optimum water content and maximum dry density tests obtained by Proctor compaction test for each group of CSA.

As can be seen from Figure 4(a), the inclusion of SSP had a clear effect on the water requirement of the CSA, with optimum water content increasing with SSP dosage. The reason may be that the specific surface area of SSP is larger than that of OPC, and the adsorption capacity of water is also stronger. However, SSP is only a small fraction of the mass of the CSA and its effect on the optimum moisture content of CSA is not significant. Even at the highest SSP blend of 50%, the optimum water content of CSA increased by only 0.22%. Regarding the maximum dry density of CSA, it showed a similar variation to the optimum moisture content. Based on the particle size distribution curve shown in Figure 2, the particle size of SSP is smaller than OPC. After using SSP

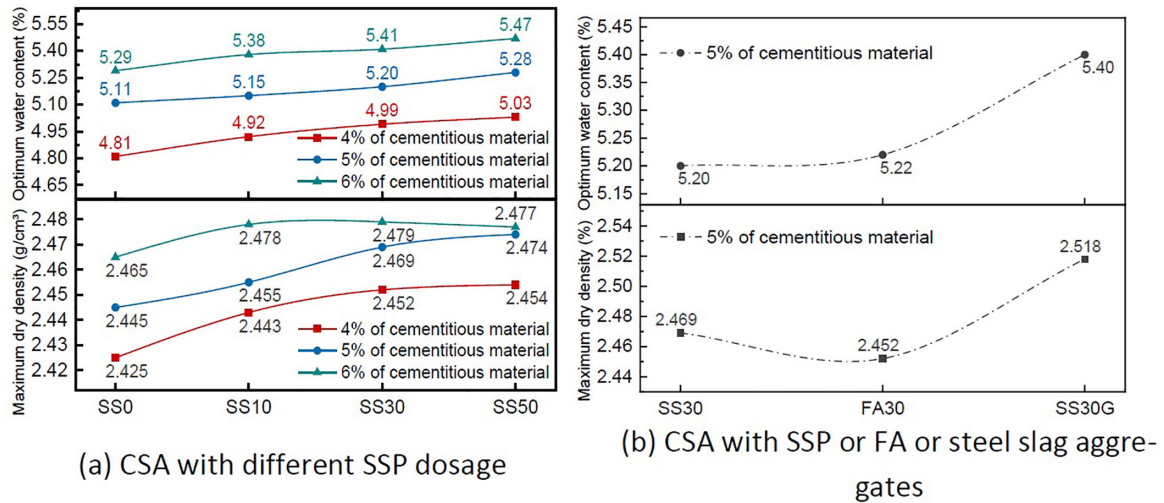


Figure 4: Test results of proctor compaction test.

to replace part of the OPC, the grading of the cementitious material of CSA was optimized to form a denser structure. From Figure 4(b), the FA30 group had a slightly higher optimum moisture content and lower maximum dry density compared to the SS30 group. This may be due to the larger particle size of FA, which results in less effective optimization of gradation compared to SSP. In addition, the optimum water content and the maximum dry density of CSA increased when SSA was incorporated, which was related to the greater water absorption and density of SSA than limestone.

3.2. Unconfined compressive strength

Figure 5 illustrates the unconfined compressive strength test results of each CSA group.

As shown in Figure 5, the SSP exhibited a positive effect, increasing the unconfined compressive strength of CSA when the SSP content was 10%. On one hand, this is due to the fact that SSP plays a role in dense filling [24]. On the other hand, SSP has a certain pozzolanic effect [25]. The active SiO_2 and Al_2O_3 it contains can lead to the secondary hydration reaction with $\text{Ca}(\text{OH})_2$ generated by the cement hydration [14]. This would facilitate the production of more high-strength calcium silicate hydrate (C-S-H) and accelerate the hydration process of unhydrated cement. For the CSA of the SS30 group with 30% SSP content, its compressive strength decreased but was still more than 6.0 MPa. This is because CSA is a semi-rigid material, and its strength comes from two aspects, including the hydration of the cementitious material and the compaction and embedment of the aggregate. The adverse effect of adding an appropriate amount of SSP on strength is limited without changing the aggregate gradation. According to the Chinese Standard JTG/T F20-2015 *Technical Guidelines for Construction of Highway Roadbases*, when CSA is used as the base layer of highway or primary highway pavement under extra heavy traffic load conditions, its compressive strength is at least 5 MPa. This shows that when the content of SSP reaches 30%, CSA still has good pavement performance. In addition, the compressive strength of the SS30 group was 0.9 MPa higher compared to that of the CSA of the FA30 group containing 30% FA. Therefore, SSP is more suitable as an admixture for CSA from the point of view of compressive strength. In terms of economy, the production of FA is declining but the consumption is growing under global initiatives aiming at energy savings and emission reduction. In some areas of China, FA sells for as much as \$40 to \$55 per ton, while steel slag powder sells for less than \$20 per ton [26]. This implies that adopting SSP also has a better cost advantage than FA. For CSA with 50% SSP content, the compressive strength decreased significantly. Only CSA with total cementitious materials of 5% and 6% can meet the strength requirements of pavement base for the highest highway grades and traffic loading conditions. This may be due to excessive SSP that causes a decrease in cement, resulting in insufficient hydration products.

It can also be seen from Figure 5 that the compressive strength of CSA of the SS30G group which was replaced by 5–10 mm crushed stone with 5–10 mm SSA decreased by 0.3 MPa compared to that of the SS30 group. This may be related to the difference in the angularity of the SSA and gravel shown in Figure 6. SSA has a more rounded appearance and is less angular than crushed stone. This may lead to a reduction in the friction area between the two aggregates and ultimately to a reduction in strength. However, the rougher surface of the SSA increases the static friction between them to some extent, compensating for the unfavorable effects caused by the poor angularity of SS. Therefore, the decrease in compressive strength of CSA of the SS30G group is small.

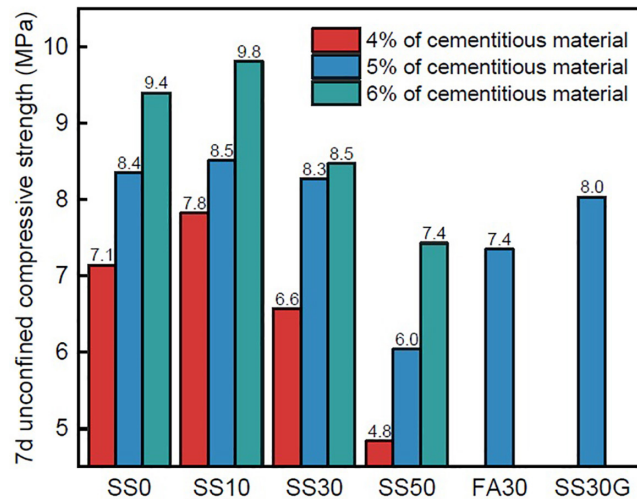


Figure 5: Unconfined compressive strength test results.



Figure 6: Morphology of SSA and limestone crushed stone.

3.3. Split tensile strength

CSA used as a pavement base is subjected to repeated vehicle loads, which can cause bending rupture when the load exceeds the limit value. In this study, the splitting tensile strength test was used to evaluate the flexural properties of CSA, and the test results are shown in Figure 7.

As can be seen in Figure 7, the splitting strength of the SS10 group with 10% SSP is slightly higher compared to the SS0 group without SSP. In general, the splitting strength of CSA depends mainly on the hydration process of the cementitious material, i.e., the level of hydration product content [27]. An appropriate amount of SSP promotes the hydration of the cement-SSP mixture, thereby improving the splitting strength of CSA. However, the splitting strength of the SS10 group only increases by 0.75% to 2.83%, which indicates that the promotion effect of SSP was weak. For CSA of SS30 and SS50 groups, the splitting strengths are 87.74%, 92.31%, 88.72% and 66.98%, 76.92%, and 74.44% when the content of cementitious materials is at 4%, 5%, and 6% respectively. This suggests that the addition of 50% SSP leads to a significant decrease in CSA splitting strength, whereas at a content of 30%, this unfavorable effect is minor. At present, the existing Chinese Standard have not given recommended values for the design value of the splitting strength under each grade of highway. According to the study of TAN [28], the splitting strength of CSA should be greater than 0.76 MPa under extra heavy traffic conditions and 0.70 MPa under heavy traffic conditions. This means that all groups of CSA with SSP content not exceeding 30% meet the splitting strength requirements under extremely heavy traffic load conditions. For CSA with 50% SSP, it is necessary to increase the amount of cementitious material to 5% or more to meet the requirement. Therefore, the SSP addition should not be too high for CSA with low-gelling

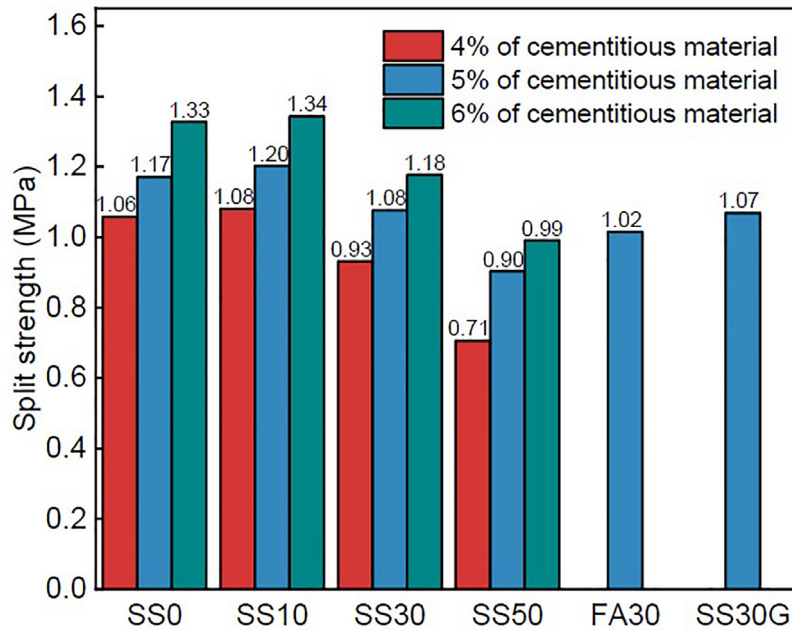


Figure 7: Splitting strength test results.

material content. In addition, the SS30 group has a higher splitting strength compared to the FA30 group, which further indicates that fly ash is not as effective as SSP in CSA. For the SS30G group, the splitting strength is only 0.01 MPa lower than that of the SS30 group, indicating that the SSA has a smaller effect on the CSA splitting strength and a larger effect on the compressive strength.

3.4. Drying shrinkage

To analyze the effect of SSP and SSA on the drying and shrinking characteristics of CSA, CSA with 5% cementitious material content was selected for the drying and shrinking test, and the results are shown in Figure 8.

As can be seen from Figure 8(a), the total water loss rate of CSA in all groups shows a trend of rapid increase followed by a slow increase and finally stabilized. A comparison of the total water loss values for each group of CSA reveals that the total water loss of CSA is greater with the increase in the incorporation of SSP and that the incorporation of SSA further increases the total water loss. Combined with the analysis in Section 3.1, it can be seen that the optimum water content of CSA shows an increasing trend with the incorporation of SSP and SS. Correspondingly, there is more water content in these samples, while SSP hydrates at a slower rate than cement [29], leading to higher free water content in CSA containing SSP and SSA, which causes an increase in its water loss rate. The FA30 group has a higher water loss rate compared to the SS30 group, which suggests that FA has a lower degree of early hydration reaction than SSP. From Figure 8(b), it can be seen that the variation of the drying shrinkage factor of each group of CSA is different from that of water loss. The coefficient of drying shrinkage decreases with the increase of SSP doping and its variation curve flattens out more quickly. At the end of the test, the maximum drying coefficients of the SS10, SS30, and SS50 groups are 141.05×10^{-6} , 114.81×10^{-6} and 98.62×10^{-6} , respectively, which are 9.96%, 26.71%, and 37.05% lower than those of the SS0 group, respectively. This suggests that SSP reduces the drying shrinkage of CSA and thus reduces the risk of cracking in CSA pavement subgrade. The reason is that the free calcium oxide in SSP can react with water to form $\text{Ca}(\text{OH})_2$ with a volume expansion effect [30, 31], which to some extent fills the pores caused by water loss in CSA and plays a role in shrinkage compensation. Comparing the SS30 and SS30G groups, it can also be found that the drying shrinkage coefficient of the SS30G group is 7.35% lower than that of the SS30 group, indicating that the addition of SSA on top of the added SSP can further improve the cracking resistance of CSA. In addition, adding FA also reduces the drying shrinkage of CSA, but it is less effective compared to the SS30 group.

3.5. Water immersion expansion

Due to the potentially expansive nature of SS, it may cause damage to the CSA pavement subgrade owing to volume expansion. In this study, an immersion swelling rate test was conducted using CSA with and without SS, respectively, and the results are shown in Figure 9.

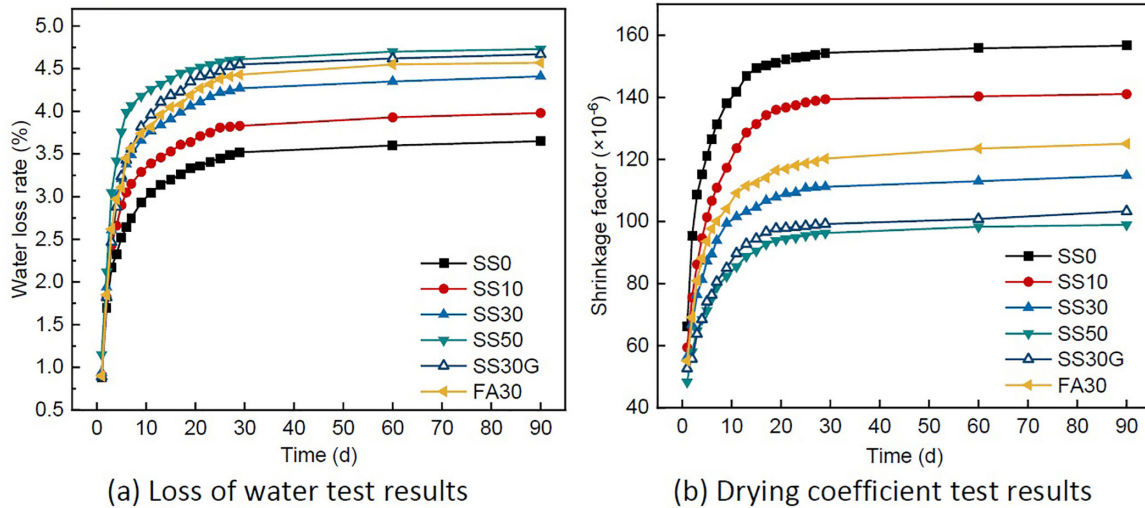


Figure 8: Drying shrinkage test results.

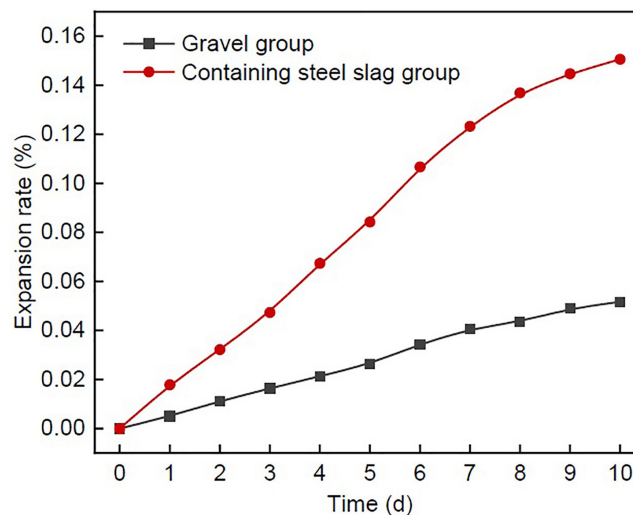


Figure 9: Results of the water immersion test.

As depicted in Figure 9, the expansion rate of CSA without SSA increases more gently, and its maximum expansion rate is only 0.052%. In contrast, the expansion rate of CSA with SSA increases significantly faster. On the 3rd day of the immersion test, its expansion rate value is close to the peak expansion rate of CSA without SS, reaching 0.047%. At the end of the experiment, the expansion rate value of CSA containing SSA is 0.151%, which is 2.9 times of CSA without SS. According to the Chinese Standard GB/T 25824-2010 *Steel Slag for Road*, the water-immersion expansion rate of SSA for road subgrade should not be more than 2%. This means that although SSA increases the expansion of CSA, it can still be used as a pavement subgrade, and drying shrinkage tests have also shown that SSA reduces the shrinkage of CSA and ensures the stability of the material. It can also be seen from Table 3 that the expansion of SSA used in this study is only 1.2%. Therefore, even using all SS, the CSA expansion will meet code requirements.

3.6. XRD analysis

In order to analyze the effect of SSP on the hydration reaction of CSA, the pure cement-SSP(CSSP) and pure cement-FA(CFA) paste samples were produced for XRD analysis in this study, and the results are shown in Figure 10.

As depicted in Figure 10, the main mineral phases of the samples in the SS0 group are $\text{Ca}(\text{OH})_2$, CaCO_3 , C_2S , and C_3S , and the addition of SSP does not change the mineral composition of the CSSP. For the CFA samples, diffraction peaks of SiO_2 appear in the XRD spectra, which is mainly caused by the quartz contained in FA.

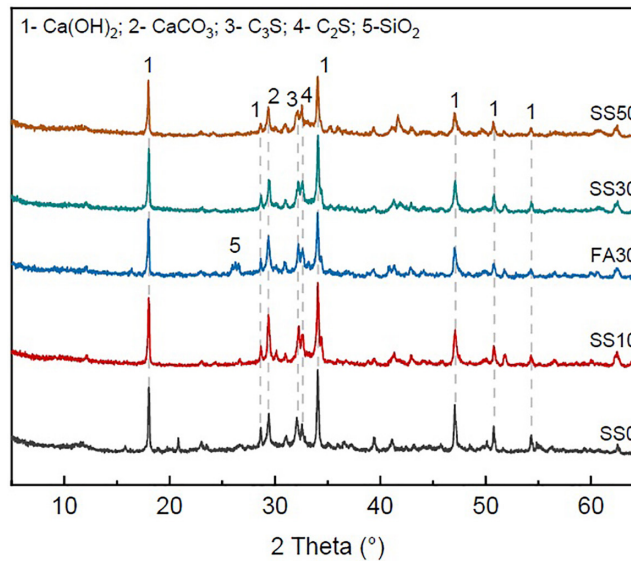


Figure 10: XRD spectra of cement-SSP and cement-FA.

Table 7: Comparison of $\text{Ca}(\text{OH})_2$ diffraction peak intensities of CSSP and CFA.

TEST NUMBER	SS0	SS10	SS30	FA30	SS50
$2\theta \approx 18^\circ$	639	657	619	574	542
$2\theta \approx 34^\circ$	801	797	740	633	576

C-S-H cannot be reflected in XRD, for it is amorphous, it. But it's worth mentioning that the hydration reaction of cement is mainly a process in which C_2S and C_3S react with water to produce $\text{Ca}(\text{OH})_2$ and C-S-H [32], which means that the higher the intensity of the diffraction peak of $\text{Ca}(\text{OH})_2$, the more adequate the hydration reaction of the cement [33]. Table 7 shows the intensity values of $\text{Ca}(\text{OH})_2$ diffraction peaks of CSSP and CFA in $2\theta \approx 18^\circ$ and $2\theta \approx 34^\circ$.

According to Table 7, compared to the SS0 group, the total diffraction peak intensity of $\text{Ca}(\text{OH})_2$ of the SS10 group slightly increases, indicating a higher degree of hydration in the SS10 group. The mechanism of action is that the volcanic ash reaction of reactive SiO_2 and Al_2O_3 in SSP consumes part of $\text{Ca}(\text{OH})_2$, and this process not only generates more C-S-H but also promotes cement hydration to generate $\text{Ca}(\text{OH})_2$. Usually, C-S-H gels are considered the main source of strength of cementitious materials [34, 35]. This explains why the mechanical strength of SS10 group CSA is higher. The intensity of $\text{Ca}(\text{OH})_2$ diffraction peaks decreases gradually with the increased addition of SSP. This indicates that excessive SSP will weaken the hydration reaction of cement, which is also basically consistent with the variation of CSA in mechanical strength. Comparing to the SS30 and FA30 groups, it can be found that the intensity of $\text{Ca}(\text{OH})_2$ diffraction peaks of the FA30 group is weaker than that of the SS30 group. This confirms that SSP is more active than FA and is more suitable as a CSA admixture.

3.7. SEM observation

The hardened cement stone formed by the hydration of the cementitious materials in the CSA is an important source of its mechanical strength. The microstructure of CSA-hardened cement stone can be observed by SEM and can also reflect its hydration degree to some extent. The SEM observation results are shown in Figure 11.

As presented in Figure 11(a,b), the hydration products of the SS0 and SS10 groups are mainly C-S-H gels and bulk $\text{Ca}(\text{OH})_2$, with very little low-strength plate-like $\text{Ca}(\text{OH})_2$, and their microstructures appear to be dense and less porous. This observation further implies a higher level of hydration. With the content of SSP up to 30%, some plate-like $\text{Ca}(\text{OH})_2$ appears in the CSA hardened cement stone, and the content of C-S-H gel decreases, while its microstructure is still relatively dense (Figure 11(c)). This may also explain the relatively small decrease in mechanical strength of SS30 group CSA. For the SS50 group with 50% SSP content, it shows a lower degree of hydration as evidenced by a further decrease in the C-S-H gel content and a significant

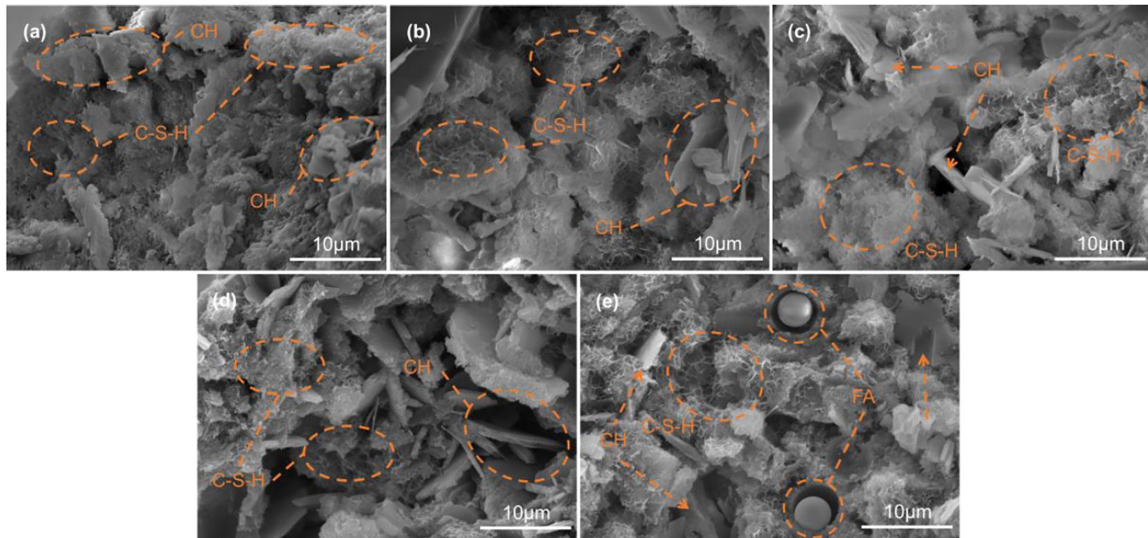


Figure 11: Microscopic morphology of CSA hardened cement stone: (a) SS0; (b) SS10; (c) SS30; (d) SS50; (e) FA30.

Table 8: CO₂ emission factor of the main components of CSA.

ITEMS	CO ₂ EMISSION FACTOR (kgCO ₂ /t)	REFERENCES
OPC	810	Literatures [36]
SSP	19	Literatures [37]
FA	27	Literatures [38]
SSA	1.01	Literatures [39]
Sand	2.51	Chinese Standard GB/T51366-2019 <i>Standard of Building Carbon Emission Calculation</i>
Gravel	2.18	

increase in plate-like Ca(OH)₂ (Figure 11(d)). These plate-like Ca(OH)₂ cannot be tightly stacked, which can easily form a large number of pores, leading to a large number of stress concentration points inside the hardened cement stone. This ultimately leads to a significant reduction in the mechanical strength of the CSA. A comparison of Figure 11(c) and Figure 11(e) reveals that the microstructures of SS30 and FA30 appear to have a similar degree of densification. However, some incompletely hydrated FA particles are also present in the FA30 group, and the presence of these particles also leads to an increase in the number of hardened cement stone pores. This may also explain the lower CSA mechanical strength of the FA30 group compared to the SS30 group.

3.8. Estimation of carbon emissions

SS is a low-carbon material, so investigating the environmental efficiency of the CSA with SS is essential. According to the existing studies, the carbon emission factor of each raw material of CSA is shown in Table 8.

In this study, CSA with 5% cementitious material content was selected for carbon emission analysis. The CO₂ emissions of CSA are determined by multiplying the mass of each raw material by its corresponding carbon emission factor. According to the raw material ratio in Table 6 and the maximum dry density data in Figure 4, the CO₂ emissions per cubic meter of CSA were calculated as shown in Figure 12.

As depicted in Figure 12, SSP has satisfactory results in reducing carbon emissions. As the proportion of SSP increases, the CO₂ emission of CSA decreases from 99.6 kgCO₂/m³ to 54.3 kgCO₂/m³, with a maximum reduction of 45.5%. This effect is due to the lower carbon emission factor of the SSP. A comparison of SS30 and FA30 shows both have similar CO₂ emissions, which indicates that they have the same effect on carbon reduction of CSA. It is worth noting that SS30G, which uses SSA with a lower carbon emission factor to replace part of the crushed stone, has higher CO₂ emissions compared to SS30. According to Figure 4, this is because SSA increases the maximum dry density of CSA, resulting in a higher amount of cement. Overall, CSA prepared by SS is a low-carbon and sustainable material owing to its cement saving, solid waste consumption, and carbon emission reduction.

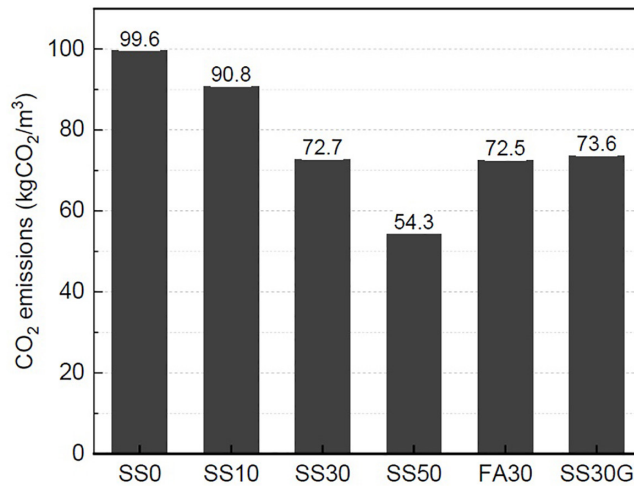


Figure 12: CO₂ emissions of CSA.

Table 9: Cost of each group of CSA with 5% binder content.

ITEMS	SS0	SS10	SS30	FA30	SS50	SS30G
Costs (\$/m ³)	21.72	21.23	20.19	20.97	19.07	19.4
Cost savings rate (%)	/	2.24	7.03	3.43	12.18	10.66
Compressive strengths (MPa)	8.4	8.5	8.3	7.4	6.0	8.0
Rate of change in strength (%)	/	+1.19	-1.19	-11.90	-28.57	-4.76

3.9. Economic benefit analysis

This study analyzed the costs of different CSA using the average prices of raw materials in Guangxi Province, China. Market research provided the following material prices: OPC (P·O 42.5) at approximately \$62/t, FA at approximately \$40/t, SSP at approximately \$15/t, Sandat approximately \$6.9/t, limestone gravel at approximately \$5.8/t, and SSA at approximately \$2/t. Then, based on the mix proportions as shown in Table 6 and the maximum dry densities as depicted in Figure 4, the costs of CSA mixes with 5% binder content were calculated. The results are presented in Table 9.

According to Table 9, the higher SSP doping, the lower the cost of CSA. Additionally, due to the low cost of SSA, substituting gravel with SSA in addition to using SSP can further reduce costs. Comparing SS30 and FA30, it is observed that incorporating SSP reduces the cost of CSA by 7.03%, whereas incorporating FA only reduces it by 3.43%. Clearly, SSP, with its lower raw material costs, offers greater cost reduction benefits compared to FA. Interestingly, the cost of SS50 group CSA decreased by 12.18%, but its compressive strength dropped significantly by 28.57%. This suggests that higher SSP content does not necessarily yield better results. Considering both cost and performance factors, for road with higher performance requirements, the appropriate proportion of SSP in CSA is 30%. Conversely, the optimal proportion of SSP is 50%.

4. CONCLUSIONS

In this study, an experimental program was conducted to investigate the effect of SS on the performance of CSA, and the mechanism of the effect was analyzed with the help of XRD and SEM. The following conclusions can be drawn:

Adding SSP and SSA increases the optimal moisture content and maximum dry density of CSA. In terms of mechanical performance, adding 10% SSP is beneficial, but excessive SSP significantly reduces mechanical properties. The optimal SSP content is 30%. Additionally, at the same additive levels, CSA containing SSP exhibits better mechanical performance than CSA containing FA.

The incorporation of SSP and SSA reduces the drying shrinkage of CSA, thereby decreasing the risk of cracking. Additionally, the water immersion expansion rate of CSA with SSA is only 0.151%, which is much lower than the 2% limit for expansion rate.

The addition of an appropriate amount of SSP can promote the hydration reaction of CSA and form a dense microstructure. CSA containing SSP shows a higher degree of hydration compared to CSA containing FA at equivalent levels, suggesting that SSP is more suitable as an admixture for CSA.

SSP demonstrates a satisfactory carbon reduction effect. When the SSP content is 30%, the CO₂ emissions of CSA decrease from 99.6 kgCO₂/m³ to 72.7 kgCO₂/m³. However, further addition of SSA does not lead to additional reductions in the CO₂ emissions of CSA. The carbon reduction effect of FA on CSA is similar to that of SSP.

The higher the doping of SSP, the lower the cost of CSA, but considering both cost and performance, the appropriate proportion of SSP in CSA is 30% when the road requires high performance. In this case, the cost saving is about 7.03%.

This study focuses solely on incorporating steel slag into CSA. However, there are numerous types of industrial solid waste. We recommend that future research explore the utilization of various industrial solid wastes such as desulfurization gypsum and red mud in CSA. This approach may potentially leverage synergistic effects among different solid wastes to improve the performance of CSA while facilitating the disposal of multiple solid wastes.

5. BIBLIOGRAPHY

- [1] CHINA NATIONAL BUREAU OF STATISTICS, “*Statistical Bulletin of the People’s Republic of China on National Economic and Social Development 2022*”, https://www.gov.cn/xinwen/2023-02/28/content_5743623.htm, accessed in June 2024.
- [2] LI, H., CUI, C., CAI, J., *et al.*, “Utilization of steel slag in road semi-rigid base: a review”, *Coatings*, v. 12, n. 7, pp. 994, 2022. doi: <http://doi.org/10.3390/coatings12070994>.
- [3] SHEEN, Y.N., WANG, H.Y., SUN, T.H., “A study of engineering properties of cement mortar with stainless steel oxidizing slag and reducing slag resource materials”, *Construction & Building Materials*, v. 40, pp. 239–245, 2013. doi: <http://doi.org/10.1016/j.conbuildmat.2012.09.078>.
- [4] YILDIRIM, I.Z., PREZZI, M., “Chemical, mineralogical, and morphological properties of steel slag”, *Advances in Civil Engineering*, v. 201, pp. 463638, 2011. doi: <http://doi.org/10.1155/2011/463638>.
- [5] ZHANG, G., WANG, S., WANG, B., *et al.*, “Properties of pervious concrete with steel slag as aggregates and different mineral admixtures as binders”, *Construction & Building Materials*, v. 257, pp. 119543, 2020. doi: <http://doi.org/10.1016/j.conbuildmat.2020.119543>.
- [6] HUMBERT, P.S., CASTRO-GOMES, J., “CO₂ activated steel slag-based materials: a review”, *Journal of Cleaner Production*, v. 208, pp. 448–457, 2019. doi: <http://doi.org/10.1016/j.jclepro.2018.10.058>.
- [7] WENG, Y., LIU, Y., LIU, J., “Study on a mathematical model of hydration expansion of steel slag-cement composite cementitious material”, *Environmental Technology*, v. 42, n. 18, pp. 2776–2783, 2021. doi: <http://doi.org/10.1080/09593330.2020.1713906>. PMID:31916506.
- [8] LIU, Q., LIU, J., QI, L., “Effects of temperature and carbonation curing on the mechanical properties of steel slag-cement binding materials”, *Construction & Building Materials*, v. 124, pp. 999–1006, 2016. doi: <http://doi.org/10.1016/j.conbuildmat.2016.08.131>.
- [9] GEORGE, C., “Slag used as an aggregate in concrete and cement-based materials”, In: WANG, G.C. *The Utilization of Slag in Civil Infrastructure Construction*, chapter 11, Sawston, Woodhead Publishing, pp. 239–274, 2016.
- [10] FISHER, L., BARRON, A., “The recycling and reuse of steelmaking slags - a review”, *Resources, Conservation and Recycling*, v. 146, pp. 244–255, 2019. doi: <http://doi.org/10.1016/j.resconrec.2019.03.010>.
- [11] ZHANG, X., CHEN, J., JIANG, J., *et al.*, “The potential utilization of slag generated from iron-and steelmaking industries: a review”, *Environmental Geochemistry and Health*, v. 42, n. 5, pp. 1321–1334, 2020. doi: <http://doi.org/10.1007/s10653-019-00419-y>. PubMed PMID: 31664635.
- [12] JOENCK, F., JOENCK, V., CARPIO, J., *et al.*, “Self-healing capacity of asphalt mixtures with steel fiber, steel slag and graphite powder, evaluated with microwave induction and fatigue test”, *Matéria (Rio de Janeiro)*, v. 27, n. 4, pp. e20220021, 2022. doi: <http://doi.org/10.1590/1517-7076-rmat-2022-0221>.

- [13] ZHUO, K.X., LIU, G.T., LAN, X.W., *et al.*, “Fracture behavior of steel slag powder-cement-based concrete with different steel-slag-powder replacement ratios”, *Materials (Basel)*, v. 15, n. 6, pp. 2243, 2022. doi: <http://doi.org/10.3390/ma15062243>. PubMed PMID: 35329694.
- [14] TIAN, E., LIU, Y., CHENG, X., *et al.*, “Characteristics of pavement cement concrete incorporating steel slag powder”, *Advances in Materials Science and Engineering*, v. 2022, pp. 6360301, 2022. doi: <http://doi.org/10.1155/2022/6360301>.
- [15] ROSLAN, N., ISMAIL, M., KHALID, N., *et al.*, “Properties of concrete containing electric arc furnace steel slag and steel sludge”, *Journal of Building Engineering*, v. 28, pp. 101060, 2020. doi: <http://doi.org/10.1016/j.job.2019.101060>.
- [16] PAN, Z., ZHOU, J., JIANG, X., *et al.*, “Investigating the effects of steel slag powder on the properties of self-compacting concrete with recycled aggregates”, *Construction & Building Materials*, v. 200, pp. 570–577, 2019. doi: <http://doi.org/10.1016/j.conbuildmat.2018.12.150>.
- [17] PASETTO, M., BALIELLO, A., GIACOMELLO, G., *et al.*, “Sustainable solutions for road pavements: a multi-scale characterization of warm mix asphalts containing steel slags”, *Journal of Cleaner Production*, v. 166, pp. 835–843, 2017. doi: <http://doi.org/10.1016/j.jclepro.2017.07.212>.
- [18] AZIZ, M., HAININ, M., YAACOB, H., *et al.*, “Characterisation and utilisation of steel slag for the construction of roads and highways”, *Materials Research Innovations*, v. 18, n. sup6, pp. 255–259, 2014. doi: <http://doi.org/10.1179/1432891714Z.000000000967>.
- [19] DONDI, G., MAZZOTTA, F., LANTIERI, C., *et al.*, “Use of steel slag as an alternative to aggregate and filler in road pavements”, *Materials (Basel)*, v. 14, n. 2, pp. 345, 2021. doi: <http://doi.org/10.3390/ma14020345>. PMID:33445570.
- [20] SHEN, A., ZHAI, C., GUO, Y., *et al.*, “Mechanism of adhesion property between steel slag aggregate and rubber asphalt”, *Journal of Adhesion Science and Technology*, v. 32, n. 24, pp. 2727–2740, 2018. doi: <http://doi.org/10.1080/01694243.2018.1507505>.
- [21] PALANKAR, N., SHANKAR, A., MITHUN, B., “Durability studies on eco-friendly concrete mixes incorporating steel slag as coarse aggregates”, *Journal of Cleaner Production*, v. 129, pp. 437–448, 2016. doi: <http://doi.org/10.1016/j.jclepro.2016.04.033>.
- [22] ALEX RAJESH, A., SENTHILKUMAR, S., SAMSON, S., “Optimal proportional combinations of rubber crumbs and steel slag for enhanced concrete split tensile strength”, *Matéria (Rio de Janeiro)*, v. 28, n. 4, pp. e20230206, 2023. doi: <http://doi.org/10.1590/1517-7076-rmat-2023-0206>.
- [23] TATARANNI, P., SANGIORGI, C., “Synthetic aggregates for the production of innovative low impact porous layers for urban pavements”, *Infrastructures*, v. 4, n. 3, pp. 4858, 2019. doi: <http://doi.org/10.3390/infrastructures4030048>.
- [24] YANG, J., LU, J., WU, Q., *et al.*, “Influence of steel slag powders on the properties of MKPC paste”, *Construction & Building Materials*, v. 159, pp. 137–146, 2018. doi: <http://doi.org/10.1016/j.conbuildmat.2017.10.081>.
- [25] ZHENG, F., LUN, Y., “Research on effect of steel slag powder and silica fume compounding on cement mortar”, *Journal of Wuhan Polytechnic University*, v. 37, n. 06, pp. 63–68, 2018.
- [26] QIU, S., DAI, D., “Effects of different aggregates on the strength of fly ash-based foam concrete”, *Journal of Shaoyang University*, v. 20, n. 03, pp. 57–66, 2023.
- [27] WANG, Q., LIANG, Y., ZHAO, Y., *et al.*, “Road performance of subgrade consisted of cement stabilized steel slag and crushed stone”, *Journal of Water Resources and Water Engineering*, v. 34, n. 1, pp. 143–151, 2023.
- [28] TAN, X., “Study on the multiple indicator quality control method of the cement stabilized macadam base”, M.Sc., Chang’an University, Xi’an, China, 2013.
- [29] WANG, Q., YAN, P., YANG, J., *et al.*, “Influence of steel slag on mechanical properties and durability of concrete”, *Construction & Building Materials*, v. 47, pp. 1414–1420, 2013. doi: <http://doi.org/10.1016/j.conbuildmat.2013.06.044>.
- [30] MARTINS, A., CARVALHO, J., COSTA, L., *et al.*, “Steel slags in cement-based composites: an ultimate review on characterization, applications and performance”, *Construction & Building Materials*, v. 291, pp. 123265, 2021. doi: <http://doi.org/10.1016/j.conbuildmat.2021.123265>.

- [31] LI, S., CHENG, S., MO, L., *et al.*, “Effects of steel slag powder and expansive agent on the properties of ultra-high performance concrete (UHPC): based on a case study”, *Materials (Basel)*, v. 13, n. 3, pp. 683, 2020. doi: <http://doi.org/10.3390/ma13030683>. PMID:32028705.
- [32] SHEN, W., “Hydration and hardening of silicate cements”, In: SHEN, W., HUANG, W., MIN, P. (eds), *Cement Processing*, chapter 8, pp. 140–171, Beijing, China, China Architecture and Building Press, 1986.
- [33] WANG, Y., ZHAO, J., SU, W., “Study on preparation and thermal conductivity of foam concrete inorganic thermal insulation materials”, *Journal of Functional Materials*, v. 54, n. 5, pp. 5101–5106, 2023.
- [34] ZHU, Z., WANG, Z., ZHOU, Y., *et al.*, “Evaluation of the nanostructure of calcium silicate hydrate based on atomic force microscopy-infrared spectroscopy experiments”, *Nanotechnology Reviews*, v. 10, n. 1, pp. 807–818, 2021. doi: <http://doi.org/10.1515/ntrev-2021-0059>.
- [35] STARR, J., SOLIMAN, E., MATTEO, E., *et al.*, “Mechanical characterization of low modulus polymer-modified calcium-silicate-hydrate (C-S-H) binder”, *Cement and Concrete Composites*, v. 124, pp. 104219, 2021. doi: <http://doi.org/10.1016/j.cemconcomp.2021.104219>.
- [36] VAN DEN HEEDE, P., DE BELIE, N., “Environmental impact and life cycle assessment (LCA) of traditional and green concretes: literature review and theoretical calculations”, *Cement and Concrete Composites*, v. 34, n. 4, pp. 431–442, 2012. doi: <http://doi.org/10.1016/j.cemconcomp.2012.01.004>.
- [37] FAN, D., ZHANG, C., LU, J., *et al.*, “Recycling of steel slag powder in green ultra-high strength concrete (UHSC) mortar at various curing conditions”, *Journal of Building Engineering*, v. 70, pp. 106361, 2023. doi: <http://doi.org/10.1016/j.jobe.2023.106361>.
- [38] ZHANG, J., TAN, H., BAO, M., *et al.*, “Low carbon cementitious materials: sodium sulfate activated ultrafine slag/fly ash blends at ambient temperature”, *Journal of Cleaner Production*, v. 280, pp. 124363, 2021. doi: <http://doi.org/10.1016/j.jclepro.2020.124363>.
- [39] ZHU, X., LI, H., WANG, F., “Quantitative analysis of environmental impacts of micro surfacing maintenance with steel slag recycling technology”, *Journal of Wuhan University of Technology (Transportation Science & Engineering)*, pp. 1–11, Feb, 2023. <https://kns.cnki.net/kcms/detail/42.1824.U.20230227.1936.016.html>, accessed in June 2024.